Acta Crystallographica Section A
Foundations of Crystallography
ISSN 0108-7673

Received 6 January 2000
Accepted 10 March 2000

Distinction of space groups ($I23$ and $I2_13$) and ($I222$ and $I2_12_12_1$) using coherent convergent-beam electron diffraction

Kenji Tsuda,[a]* Koh Saitoh,[a] Masami Terauchi,[a] Michiyoshi Tanaka[a] and Peter Goodman[b]†

[a]Research Institute for Scientific Measurements, Tohoku University, Sendai 980-8577, Japan, and [b]School of Physics, University of Melbourne, Parkville, Victoria 3052, Australia. Correspondence e-mail: tsuda@rism.tohoku.ac.jp

Convergent-beam electron diffraction (CBED) is well known as a powerful tool to determine space groups of crystals. However, it cannot distinguish several sets of space groups. It is shown theoretically that the coherent CBED method can distinguish between space groups ($I23$ and $I2_13$) and between ($I222$ and $I2_12_12_1$), which belong to indistinguishable sets. It is demonstrated by computer simulations that the relative arrangement of 2-fold-rotation and 2_1-screw axes can be distinguished by examining the relative phases of specific reflections through the interference fringes of coherent CBED patterns. This fact implies that these space groups can be distinguished by the coherent CBED method.

1. Introduction

It has been established that convergent-beam electron diffraction (CBED) is an effective method for determining crystal point groups and space groups. CBED, based fully upon dynamical diffraction, can distinguish polar crystals from nonpolar crystals by inspecting the symmetries appearing in CBED discs, thus allowing the unique identification of all the point groups (Goodman, 1975; Tinnappel, 1975; Buxton *et al.*, 1976; Tanaka, Saito & Sekii, 1983; Tanaka, 1989). Furthermore, CBED can distinguish 2_1 screw axes and glide planes from rotation axes and mirror planes using Gjønnes–Moodie (G–M) lines or dynamical extinction lines (Gjønnes & Moodie, 1965; Tanaka, Sekii & Nagasawa, 1983; Tanaka, 1989; Tanaka & Terauchi, 1985; Tanaka *et al.*, 1988). By an examination of whether or not G–M lines are formed in kinematically forbidden reflections, most space groups among all the 230 space groups can be identified. The method using G–M lines cannot distinguish 23 sets of space groups (Table 1) (Tanaka, 1989; Tanaka *et al.*, 1988), most of the indistinguishable sets having 4_2, 3_1 (3_2) and 6_2 (6_4) screw axes, which do not produce G–M lines.

There is, however, a practical method to distinguish a rotation axis and a screw axis. The method is to observe the changes of the intensities of kinematically forbidden reflections by tilting the incident beam so that *Umweganregung* paths to the reflections disappear. By this test, each space group of an indistinguishable pair can be identified except the pairs in parentheses and the underlined special pairs in Table 1. The pairs in parentheses form left- and right-handed space groups. Identifications of the handedness of space groups were reported for quartz by Goodman & Secomb (1977) and Goodman & Johnson (1977), and for MnSi by Tanaka *et al.* (1985). The senses of the first and second crystal axes of these space groups were determined with the aid of kinematical structure-factor calculations, and the sense of the third crystal axis was determined by dynamical intensity calculations. The underlined special pairs of ($I23$ and $I2_13$) and ($I222$ and

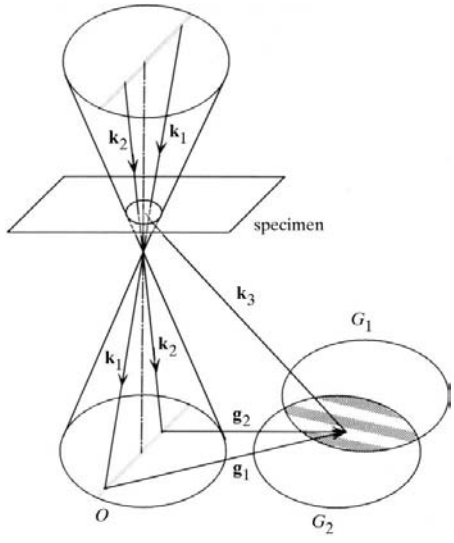

Figure 1
Ray-path diagram of the coherent CBED method. Interference fringes are seen in the overlapping regions of adjacent reflection discs.

† Tragically, Dr Peter Goodman died before this work could be published.

$I2_12_12_1$) cannot be distinguished by the above methods because these pairs show the same kinematical extinction and no dynamical extinction lines. These two special pairs have remained indistinguishable. A method to detect the phases of the structure factors is needed to distinguish the special pairs.

Coherent CBED, which uses a highly coherent electron source (*i.e.* field-emission gun), is a method to directly provide phase information on crystal structure factors. The coherent CBED technique produces interference fringes in the overlapping regions of CBED discs. From the relative positions of the fringes, the phase differences between two diffraction waves can be determined.

In the present paper, we show for the first time that the coherent CBED method can distinguish the special pairs of ($I23$ and $I2_13$) and of ($I222$ and $I2_12_12_1$). That is, a method to distinguish the space groups is proposed by demonstrating simulations of coherent CBED patterns for model structures belonging to the space groups.

Table 1
Space groups indistinguishable by dynamical extinction lines.

1. $P3$, ($P3_1$, $P3_2$)	2. $P312$, ($P3_112$, $P3_212$)	3. $P321$, ($P3_121$, $P3_221$)
4. $P6$, ($P6_2$, $P6_4$)	5. $P622$, ($P6_222$, $P6_422$)	6. $P6_3$, ($P6_1$, $P6_5$)
7. $P6_322$, ($P6_122$, $P6_522$)	8. $P4$, $P4_2$	9. ($P4_1$, $P4_3$)
10. $P4/m$, $P4_2/m$	11. $P4/n$, $P4_2/n$	12. $P422$, $P4_222$
13. $P42_12$, $P4_22_12$	14. $I4$, $I4_1$	15. $I422$, $I4_122$
16. $I23$, $I2_13$	17. $I222$, $I2_12_12_1$	18. $P432$, $P4_232$
19. ($P4_132$, $P4_332$)	20. $I432$, $I4_132$	21. $F432$, $F4_132$
22. ($P4_122$, $P4_322$)	23. ($P4_12_12$, $P4_32_12$)	

2. Coherent CBED

Experimental observations of interference fringes in coherent CBED patterns have been reported (Dowell & Goodman,

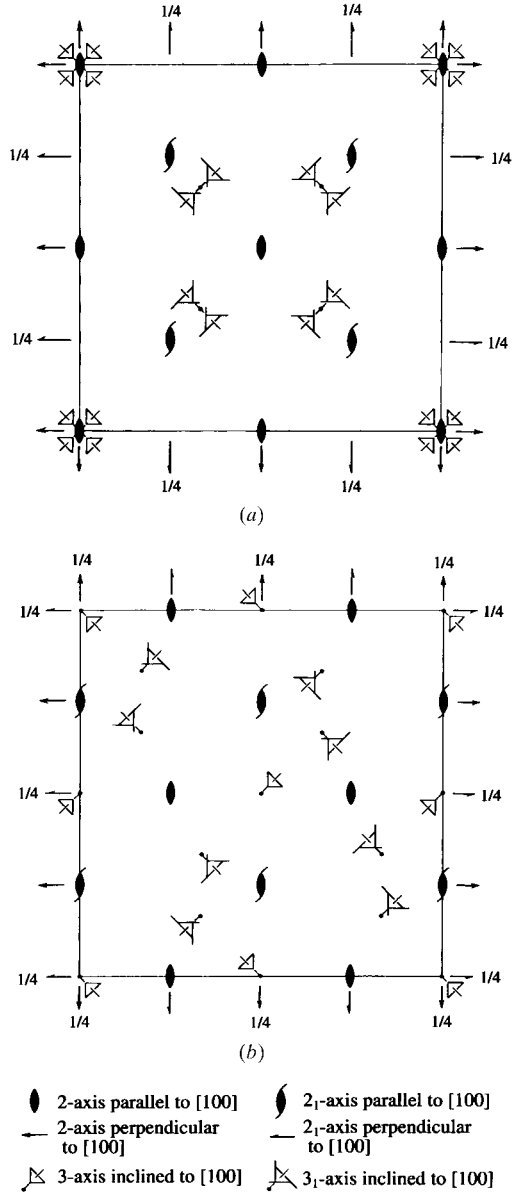

Figure 2
Arrangements of symmetry elements of (*a*) $I23$ and (*b*) $I2_13$ projected along the [100] zone axis (*International Tables for Crystallography*, 1989, Vol. A).

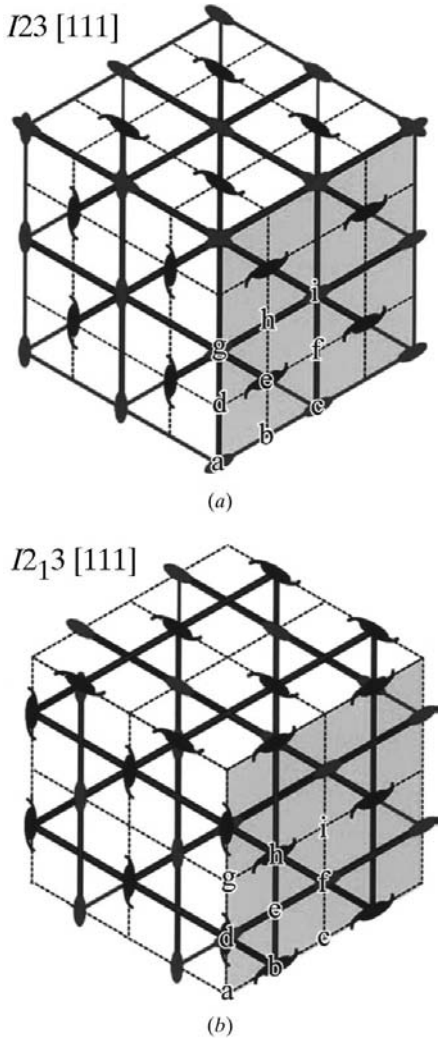

Figure 3
Arrangements of 2-fold-rotation and 2_1-screw axes of (*a*) $I23$ and (*b*) $I2_13$ projected along the [111] direction.

1973; Cowley, 1979; Vine *et al.*, 1992; Terauchi *et al.*, 1994; Tanaka *et al.*, 1994; Tsuda *et al.*, 1994; Tsuda & Tanaka, 1996; McCallum & Rodenburg, 1993; Steeds *et al.*, 1995). Formation of the interference fringes was explained in detail first by Cowley (1979), followed by Vine *et al.* (1992) and Terauchi *et al.* (1994). Local site-symmetry information appearing in coherent CBED patterns was discussed by Spence (1978), Cowley (1979), Ou & Cowley (1988) and Zuo & Spence (1993). In fact, the interference appearing in the overlapping regions of coherent CBED patterns is the basis of lattice imaging of the scanning transmission electron microscope (STEM) (Spence & Cowley, 1978). The coherent CBED method was applied to the calibration of the operating parameters of a STEM (Cowley, 1979), ptychographical phase determination (McCallum & Rodenburg, 1993), detection of a 2_1 screw axis (Steeds *et al.*, 1995) and interferometry of a stacking fault (Tsuda & Tanaka, 1996).

The geometry of coherent CBED is shown in Fig. 1. The convergence angle of the incident beam is set to a larger value than the usual one to make adjacent CBED discs overlap. At a point with wavevector $\mathbf{k}_3$ in the overlapping region of CBED discs G_1 and G_2, two waves are superposed, which are diffracted by $\mathbf{g}_1$ and $\mathbf{g}_2$, respectively, from the incident waves of $\mathbf{k}_1$ and $\mathbf{k}_2$.

If the focus point of the incident beam is on the specimen, each overlapping region of the CBED discs shows uniform intensity. When the focus point is displaced from the specimen, or a certain area is illuminated, sinusoidal interference fringes are formed in the overlapping regions (Terauchi *et al.*, 1994; Tanaka *et al.*, 1994). A shift of the probe position leads to a shift of the entire set of the interference fringes in the overlapping regions. This is described by adding a phase factor $\exp(-2\pi i\mathbf{g}\cdot\Delta\mathbf{r})$ to the structure factor of each reflection (Terauchi *et al.*, 1994; Tanaka *et al.*, 1994), where $\mathbf{g}$ is the reciprocal-lattice vector and $\Delta\mathbf{r}$ is the displacement of the probe position from the origin of the unit cell.

When the difference between the phases of the reflections $\mathbf{g}_1$ and $\mathbf{g}_2$ is 0, the waves of the reflections are added in phase at the center of the overlapping area, showing a bright fringe. When the phase difference between the two reflections is π, the center shows a dark fringe. Thus, the phase difference of the two adjacent reflections can be measured by analyzing the fringe contrast of overlapping regions.

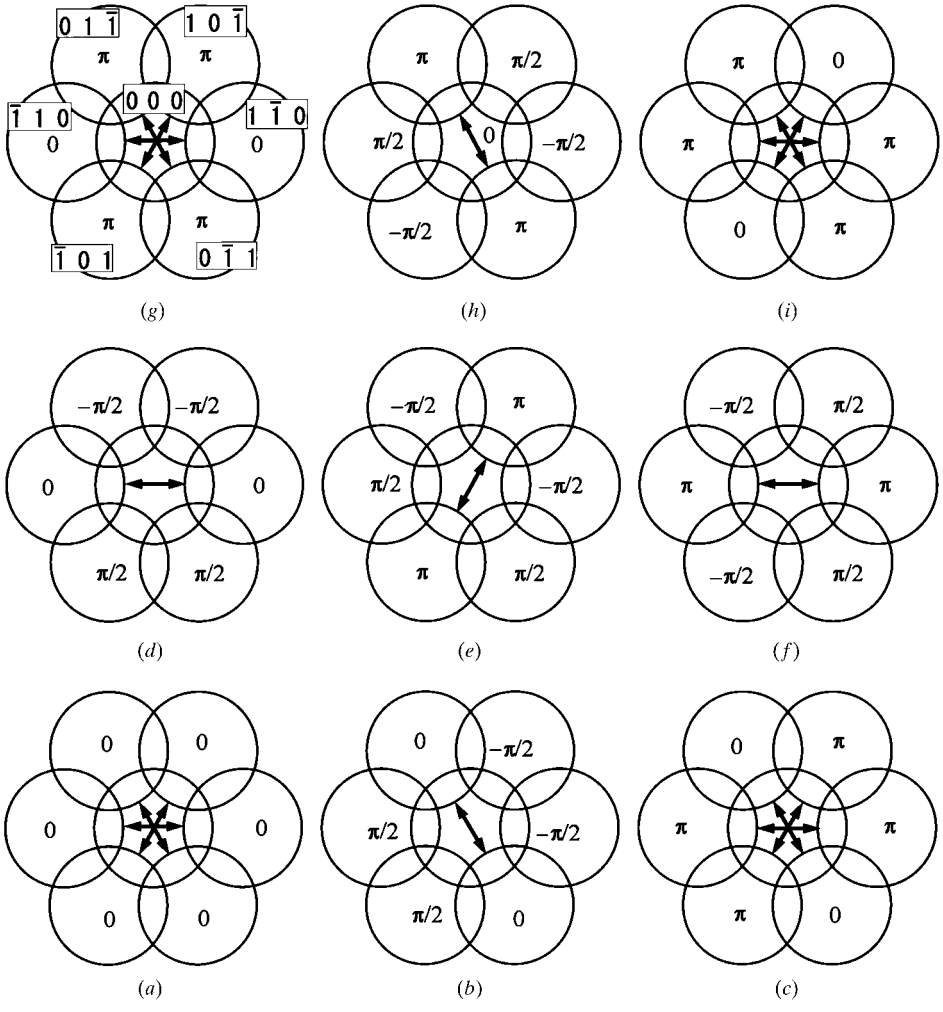

Figure 4
Phases of the kinematical crystal structure factors of the *I*23 model of Table 3 for the electron probe positions (*a*)–(*i*) illustrated in Fig. 3(*a*).

3. Determination of space groups

3.1. Space groups $I23$ and $I2_13$

First we focus our attention on the space-group pair $I23$ and $I2_13$ for convenience. It will be shown later that the same procedure can be applied to the indistinguishable space groups $I222$ and $I2_12_12_1$ because they are identical, respectively, with space groups $I23$ and $I2_13$ with respect to the arrangements of 2-fold-rotation and 2_1-screw axes.

Figs. 2(*a*) and 2(*b*) illustrate the arrangements of symmetry elements of the space groups $I23$ and $I2_13$ in projection along the [100] direction (*International Tables for Crystallography*, 1989, Vol. A). It should be noted that the space groups have both 2-fold-rotation and 2_1-screw axes (hereafter referred to as 2 and 2_1 axes) irrespective of their symbols $I23$ and $I2_13$. These space groups have the same relative arrangements of the 2 and 2_1 axes parallel to the [100] zone axis, as is seen in Fig. 2. These space groups are only distinguishable when the three-dimensional arrangements of these axes in the [100], [010] and [001] directions are examined. For example, space group $I23$ has positions at which three perpendicular 2 axes

Table 2
Atom coordinates of the general positions, relations between the structure factors and kinematical extinction rules for the space groups (*a*) $I23$ and (*b*) $I2_13$.

(*a*) $I23$
Atom coordinates:
$(0, 0, 0; \frac{1}{2}, \frac{1}{2}, \frac{1}{2})+$
$|x, y, z; x, \bar{y}, \bar{z}; \bar{x}, y, \bar{z}; \bar{x}, \bar{y}, z; y, z, x; y, \bar{z}, \bar{x}; \bar{y}, z, \bar{x}; \bar{y}, \bar{z}, x; z, x, y;$
$z, \bar{x}, \bar{y}; \bar{z}, x, \bar{y}; \bar{z}, \bar{x}, y|$
Relations between structure factors:
$|F(hkl)| = |F(\bar{h}kl)| = |F(h\bar{k}l)| = |F(hk\bar{l})| = |F(hkl)|$
$\alpha(hkl) = \alpha(\bar{h}kl) = \alpha(h\bar{k}l) = \alpha(hk\bar{l})$
Kinematical extinction rules (possible reflections):
$h + k + l = 2n$

(*b*) $I2_13$
Atom coordinates:
$(0, 0, 0; \frac{1}{2}, \frac{1}{2}, \frac{1}{2})+$
$|x, y, z; \frac{1}{2}+x, \frac{1}{2}-\bar{y}, \bar{z}; \bar{x}, \frac{1}{2}+y, \frac{1}{2}-\bar{z}; \frac{1}{2}-\bar{x}, \bar{y}, \frac{1}{2}+z;$
$y, z, x; \frac{1}{2}+y, \frac{1}{2}-z, x; \bar{y}, \frac{1}{2}+z, \frac{1}{2}-x; \frac{1}{2}-y, \bar{z}, \frac{1}{2}+x;$
$z, x, y; \frac{1}{2}+z, \frac{1}{2}-x, \bar{y}; \bar{z}, \frac{1}{2}+x, \frac{1}{2}-y; \frac{1}{2}-z, \bar{x}, \frac{1}{2}+y|$
Relations between structure factors:
$\alpha(hkl) = -\alpha(\bar{h}k\bar{l}) = -\alpha(\bar{h}kl) = -\alpha(h\bar{k}l) = -\alpha(hk\bar{l})$: h, k, l all even
$\alpha(hkl) = -\alpha(h\bar{k}\bar{l}) = \pi - \alpha(\bar{h}kl) = -\alpha(\bar{h}k\bar{l}) = \pi - \alpha(\bar{h}\bar{k}l)$: h even, k and l odd
$\alpha(hkl) = -\alpha(\bar{h}k\bar{l}) = \pi - \alpha(\bar{h}kl) = \pi - \alpha(h\bar{k}l) = -\alpha(h\bar{k}\bar{l})$: k even, l and h odd
$\alpha(hkl) = -\alpha(\bar{h}\bar{k}l) = -\alpha(\bar{h}kl) = \pi - \alpha(h\bar{k}l) = \pi - \alpha(h\bar{k}\bar{l})$: l even, h and k odd
Kinematical extinction rules (possible reflections):
$h + k + l = 2n$

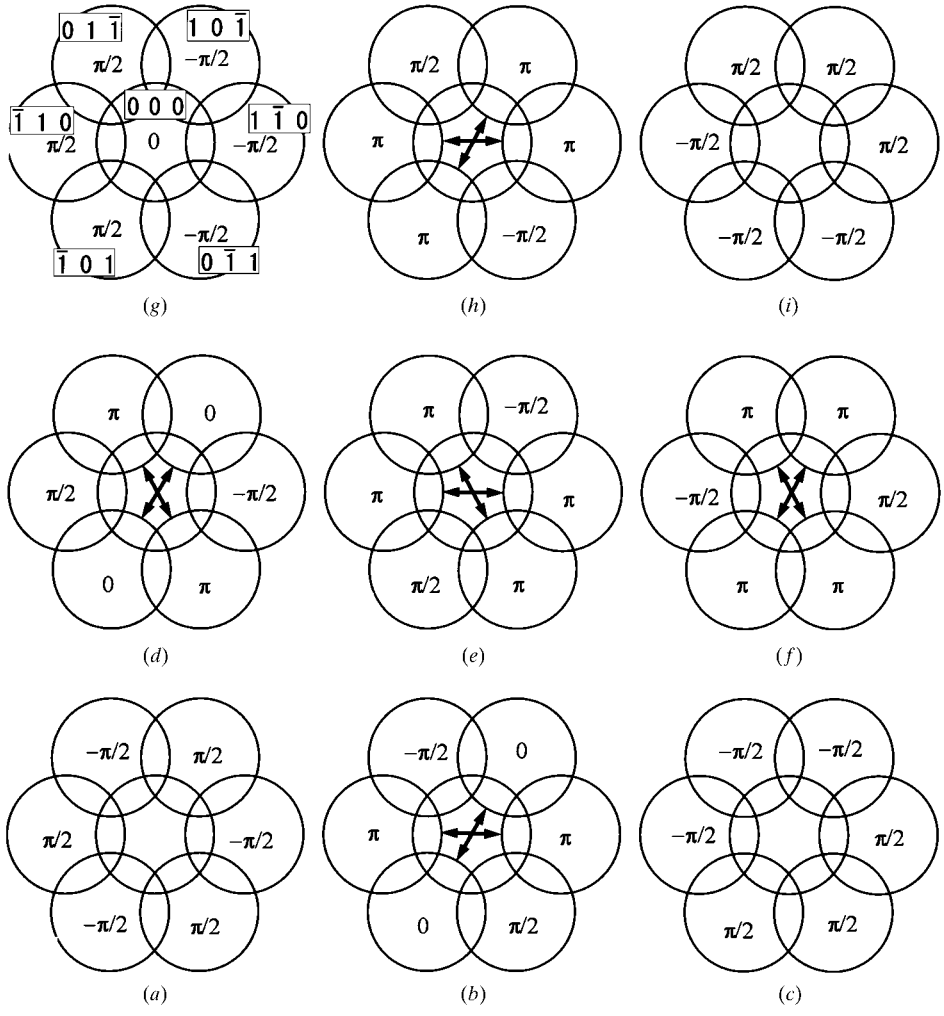

Figure 5
Phases of the kinematical crystal structure factors of the $I2_13$ model of Table 3 for the electron probe positions (*a*)–(*i*) illustrated in Fig. 3(*b*).

intersect and three perpendicular 2_1 axes also intersect, whereas $I2_13$ has no such position.

Table 2 shows atom coordinates of the general positions, relations between the structure factors and kinematical extinction rules for space groups $I23$ and $I2_13$ (*International Tables for X-ray Crystallography*, 1952, Vol. I). The relations between the phases of the structure factors are seen to be different although the kinematical extinction rules are identical for the two space groups.

The [111] zone axis is selected as a direction suitable for examining the difference of the three-dimensional arrangements of 2 and 2_1 axes between the two space groups. Figs. 3(*a*) and 3(*b*) show the arrangements of 2 and 2_1 axes in projection along the [111] direction. The solid lines in Fig. 3 indicate the 2 and 2_1 axes, which are hereafter abbreviated as $2(2_1)$ axes, because both the 2 and 2_1 axes are projected along [111]. It is clearly seen in this direction that the three perpendicular $2(2_1)$ axes intersect at the same positions (*a*, *c*, *g* and *i*) for $I23$, but only two of them intersect at the positions *b*, *d*, *e*, *f* and *h* for $I2_13$. Unfortunately, these $2(2_1)$ axes do not produce any symmetry in the conventional CBED patterns taken with [111] incidence because the $2(2_1)$ axes are neither parallel nor perpendicular to the [111] direction. On the contrary, it will be shown in the following that the coherent CBED technique can directly reveal the difference of the relative arrangement of $2(2_1)$ axes.

Table 3
Model structures of $I23$ and $I2_13$ used for simulations of coherent CBED patterns.

Space group	Site	(x,y,z)	Element	Lattice parameter (nm)
$I23$	24(f)	(0.05,0.10,0.15)	Si	a = 0.4
$I2_13$	24(c)	(0.05,0.10,0.15)	Si	a = 0.4

Table 3 shows the model structures of space groups $I23$ and $I2_13$, which are used for simulations of coherent CBED patterns. These atom positions are generated from an atom

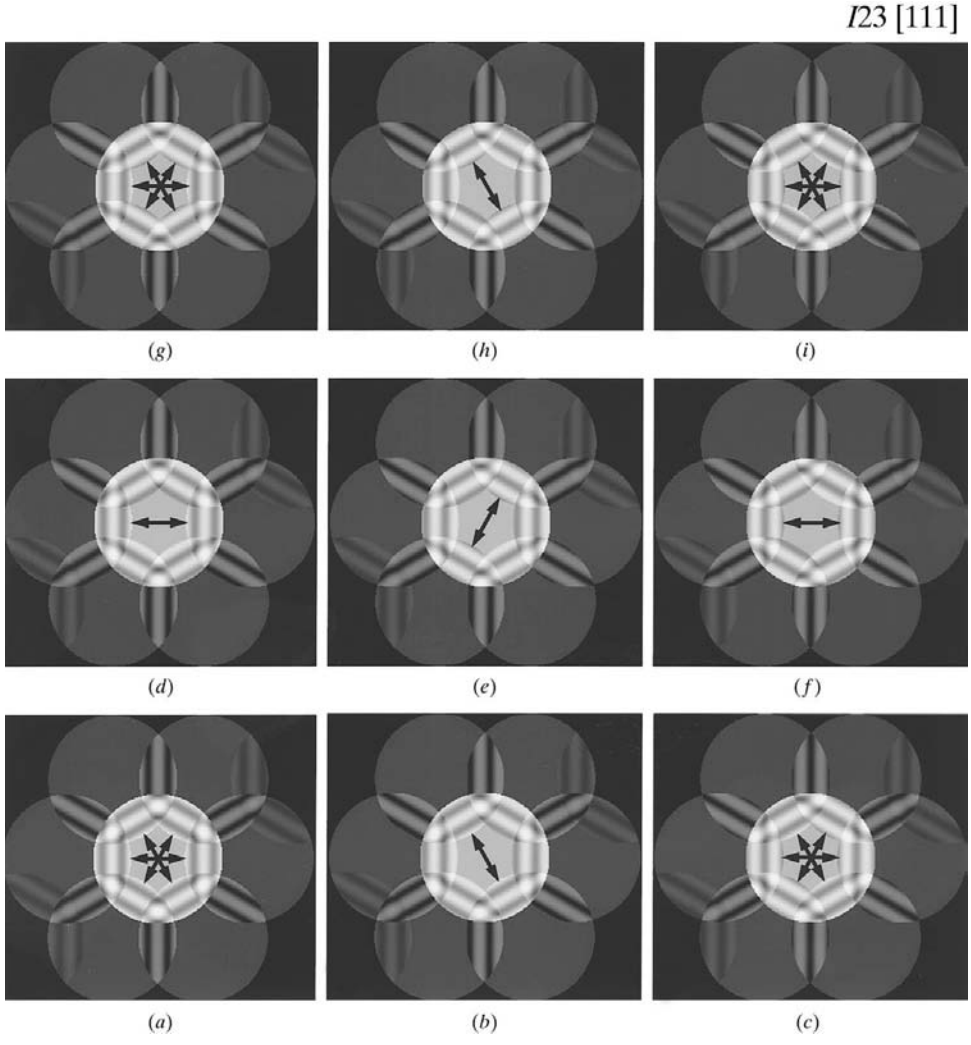

Figure 6
Coherent CBED patterns simulated for the $I23$ model for the electron probe positions (*a*)–(*i*) of Fig. 4. The pairs of overlapping areas with the same contrast are indicated by pairs of arrows. (*a*), (*c*), (*g*) and (*i*) exhibit three sets of such pairs, confirming the intersection of three perpendicular $2(2_1)$ axes at positions *a, c, g* and *i* in Fig. 3(*a*).

located at a general position (0.05,0.10,0.15) by the symmetry operation of each space group. Figs. 4(*a*)–4(*i*) show the phases of kinematical crystal structure factors of the *I*23 model in the corresponding reflection discs for the electron probe positions (*a*)–(*i*) illustrated in Fig. 3(*a*), where the relative phases depending on the probe positions, $\exp(-2\pi i\mathbf{g}\cdot\Delta\mathbf{r})$, are added to the phases of the structure factors. Figs. 5(*a*)–5(*i*) similarly show the phases of kinematical structure factors calculated for the $I2_13$ model structure. It should be noted that, when the electron probe is placed on the $2(2_1)$ axes, the structure factors of the reflections **g** and $-\mathbf{g}$ perpendicular to the axes have the same phase. This is caused by the fact that the reflections **g** and $-\mathbf{g}$ are equivalent with respect to the $2(2_1)$ axes. For example, Fig. 4(*d*), for which the probe is placed on the $2(2_1)$ axes parallel to the *c* axis, shows that reflections $1\bar{1}0$ and $\bar{1}10$ related by the $2(2_1)$ axes have the same phase π. Figs. 4(*a*), 4(*c*), 4(*g*) and 4(*i*), for which the three perpendicular $2(2_1)$ axes intersect, show that three pairs of $\pm\mathbf{g}$ reflections each have the same phase. On the other hand, there is no such intersecting position in Fig. 5. Figs. 5(*b*), 5(*d*), 5(*e*), 5(*f*) and 5(*h*), for which the only two $2(2_1)$ axes intersect, show that two pairs of $\pm\mathbf{g}$ reflections each have the same phase.

Figs. 6(*a*)–6(*i*) show coherent CBED simulation patterns for the *I*23 model, which were calculated under the kinematical approximation with a certain defocus of the illumination respectively for the electron-probe positions of Figs. 4(*a*)–4(*i*). It is noted that the interference fringes agree well with those calculated by the dynamical theory if the specimen thickness is thinner than about 10 nm for an accelerating voltage of 100 kV. In Fig. 6, the pairs of the overlapping areas with the same contrast indicated by pairs of arrows have the same phase and amplitude of the structure factors, indicating the existence of $2(2_1)$ axes. Figs. 6(*a*), 6(*c*), 6(*g*) and 6(*i*) exhibit three sets of such pairs, confirming the intersection of three perpendicular $2(2_1)$ axes at positions *a*, *c*, *g* and *i* in Fig. 3(*a*).

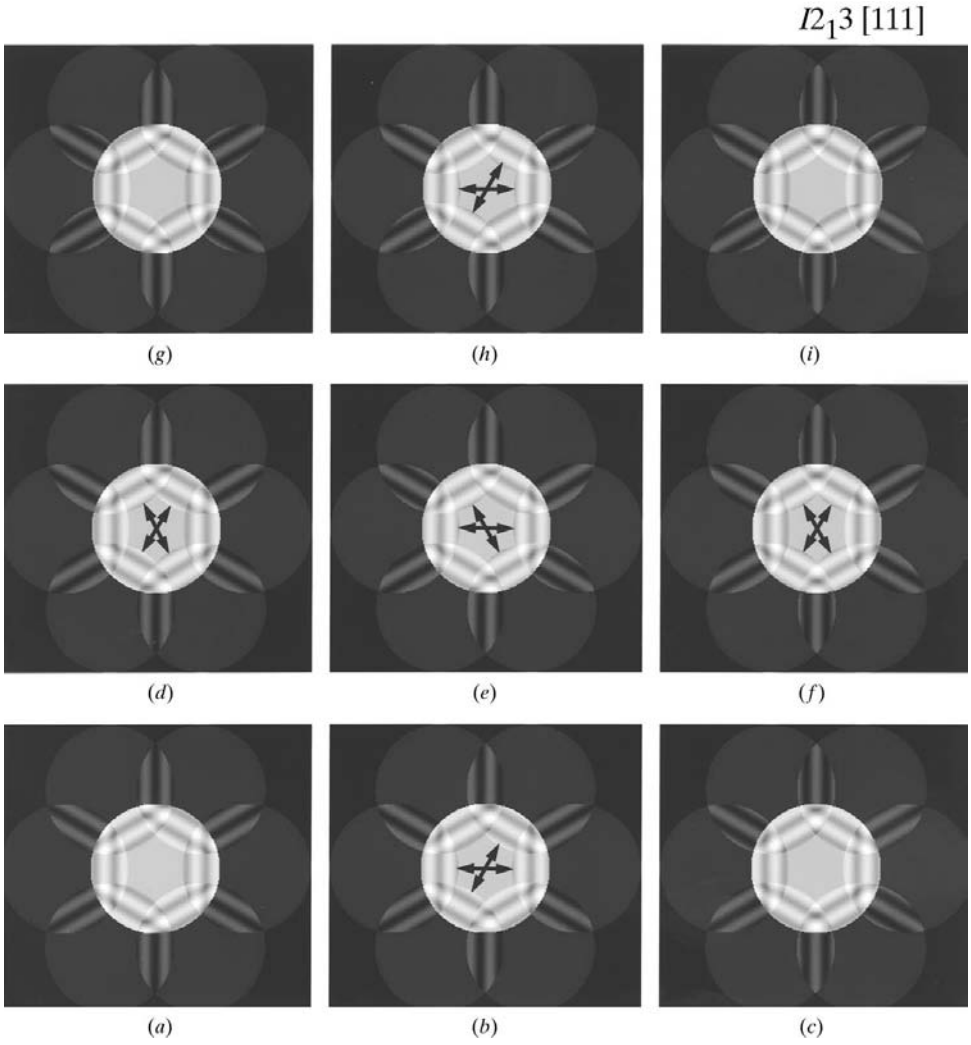

Figure 7
Coherent CBED patterns simulated for the $I2_13$ model for the electron probe positions (*a*)–(*i*) of Fig. 5. The pairs of overlapping areas with the same contrast are indicated by pairs of arrows. Only two sets of such pairs are seen in (*b*), (*d*), (*e*), (*f*) and (*h*), indicating the absence of intersection of three perpendicular $2(2_1)$ axes.

Figs. 7(*a*)–7(*i*) show coherent CBED patterns of the $I2_13$ model calculated for the electron probe positions of Figs. 5(*a*)–5(*i*), respectively. Similarly to Fig. 6, the pairs of the overlapping areas with the same contrast are indicated by pairs of arrows. In contrast to Fig. 6, there are no patterns that have three such pairs simultaneously, but only two such pairs are seen in Figs. 7(*b*), 7(*d*), 7(*e*), 7(*f*) and 7(*h*), indicating the absence of intersection of three perpendicular $2(2_1)$ axes.

Therefore, the space groups $I23$ and $I2_13$ can be distinguished by using [111] coherent CBED patterns. If the [111] coherent CBED pattern shows the three pairs of interference fringes in overlapping regions each with the same contrast, the space group is $I23$. If the pattern shows only two such pairs, then the space group is $I2_13$.

3.2. Space groups $I222$ and $I2_12_12_1$

The same examination stands for the other indistinguishable pair of space groups $I222$ and $I2_12_12_1$.

Fig. 8 illustrates the arrangements of 2 and 2_1 axes of the space groups $I222$ and $I2_12_12_1$ in projection along the [100] direction (*International Tables for Crystallography*, 1989, Vol. A). They are identical with those of the space groups $I23$ and $I2_13$ of Fig. 2 except for the absence of threefold rotation axes. Table 4 shows atom coordinates of the general positions, relations between the structure factors and kinematical extinction rules for the space groups $I222$ and $I2_12_12_1$ (*International Tables for X-ray Crystallography*, 1952, Vol. I).

Similar to the case of $I23$ and $I2_13$, [111] coherent CBED patterns were simulated using the model structures shown in Table 5. Figs. 9(*a*) and 9(*b*) show the arrangements of 2 and 2_1 axes in projection along the [111] direction. Figs. 10 and 11 illustrate the phases of the structure factors calculated for the model structures. Figs. 12 and 13 show the simulated coherent CBED patterns for the $I222$ and $I2_12_12_1$ models. The pairs of overlapping regions with the same contrast are indicated by pairs of arrows, which result from the electron probe being placed on the $2(2_1)$ axes. Three such pairs, each with the same contrast, are seen in Figs. 12(*a*), 12(*c*), 12(*g*) and 12(*i*) for space group $I222$. On the other hand, no patterns are seen that show three such pairs, but the patterns with only two such pairs are seen in Figs. 13(*b*), 13(*d*), 13(*e*), 13(*f*), 13(*h*). Therefore, similar to the case of $I23$ and $I2_13$, the space groups $I222$ and $I2_12_12_1$ can be distinguished by observing [111] coherent CBED patterns.

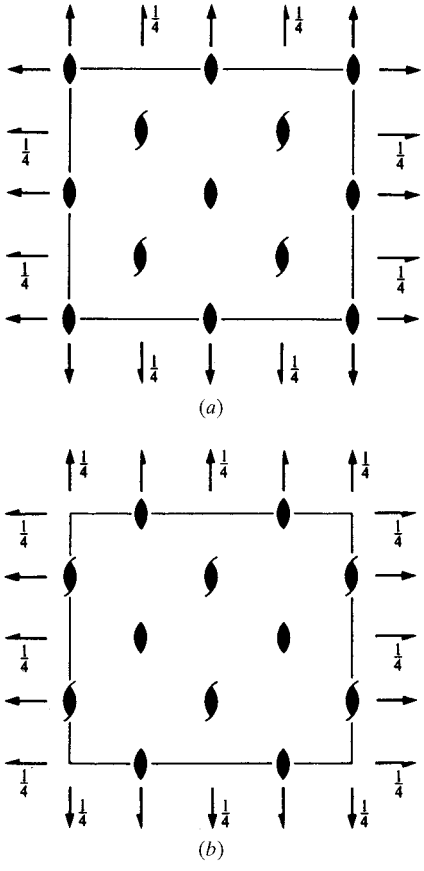

Figure 8
Arrangements of 2 and 2_1 axes of (*a*) $I222$ and (*b*) $I2_12_12_1$ projected along the [100] direction (*International Tables for Crystallography*, 1989, Vol. A).

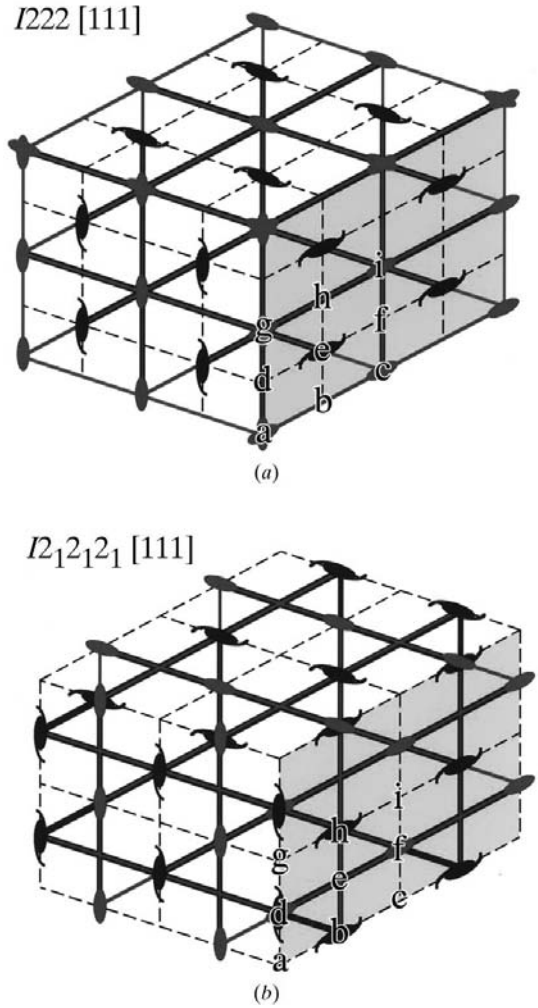

Figure 9
Arrangements of 2-fold-rotation and 2_1-screw axes of (*a*) $I222$ and (*b*) $I2_12_12_1$ projected along the [111] direction.

Table 4
Atom coordinates of the general positions, relations between the structure factors and kinematical extinction rules for the space groups (*a*) *I*222 and (*b*) $I2_12_12_1$.

(*a*) *I*222
Atom coordinates:
$(0, 0, 0; \frac{1}{2}, \frac{1}{2}, \frac{1}{2}) + |x, y, z; x, \bar{y}, \bar{z}; \bar{x}, y, \bar{z}; \bar{x}, \bar{y}, z|$
Relations between structure factors:
$|F(hkl)| = |F(\bar{h}\bar{k}l)| = |F(\bar{h}kl)| = |F(h\bar{k}\bar{l})| = |F(hkl)|$
$\alpha(hkl) = \alpha(\bar{h}\bar{k}l) = \alpha(\bar{h}kl) = \alpha(h\bar{k}\bar{l}) = \alpha(hk\bar{l})$
Kinematical extinction rules (possible reflections):
$h + k + l = 2n$

(*b*) $I2_12_12_1$
Atom coordinates:
$(0, 0, 0; \frac{1}{2}, \frac{1}{2}, \frac{1}{2}) + |x, y, z; \frac{1}{2}+x, \frac{1}{2}-y, \bar{z}; \bar{x}, \frac{1}{2}+y, \frac{1}{2}-z; \frac{1}{2}-x, \bar{y}, \frac{1}{2}+z|$
Relations between structure factors:
$\alpha(hkl) = -\alpha(\bar{h}\bar{k}l) = -\alpha(\bar{h}kl) = \pi - \alpha(h\bar{k}l) = \pi - \alpha(hk\bar{l})$: l even, h and k odd
$\alpha(hkl) = -\alpha(\bar{h}\bar{k}l) = \pi - \alpha(\bar{h}kl) = \pi - \alpha(h\bar{k}\bar{l}) = -\alpha(hk\bar{l})$: k even, l and h odd
$\alpha(hkl) = -\alpha(\bar{h}\bar{k}l) = \pi - \alpha(\bar{h}kl) = -\alpha(h\bar{k}l) = \pi - \alpha(hk\bar{l})$: h even, k and l odd
$\alpha(hkl) = -\alpha(\bar{h}\bar{k}l) = -\alpha(\bar{h}kl) = -\alpha(h\bar{k}\bar{l}) = -\alpha(hk\bar{l})$: h, k, l all even
Kinematical extinction rules (possible reflections):
$h + k + l = 2n$

4. Discussion

In the previous section, coherent CBED patterns were calculated for the model structures of Tables 3 and 4. If a model that has different atom positions and/or different atom numbers is considered, the values of the phases of structure factors change. As a result, the different contrast of the interference fringes of the coherent CBED patterns appear. However, if the probe is positioned on $2(2_1)$ axes, the phases of **g** and $-$**g** reflections perpendicular to the axes are kept the same irrespective of the model structure. Therefore, the present method can be applied to all structures with these space groups.

The possibilities of the distinction between the space groups at the [100] and [110] crystal settings are discussed in the following: The arrangements of symmetry elements of the space groups *I*23 and $I2_13$ in projection along the [100] direction have already been shown in Fig. 2. In the case of *I*23, the three perpendicular 2 axes intersect at the same positions

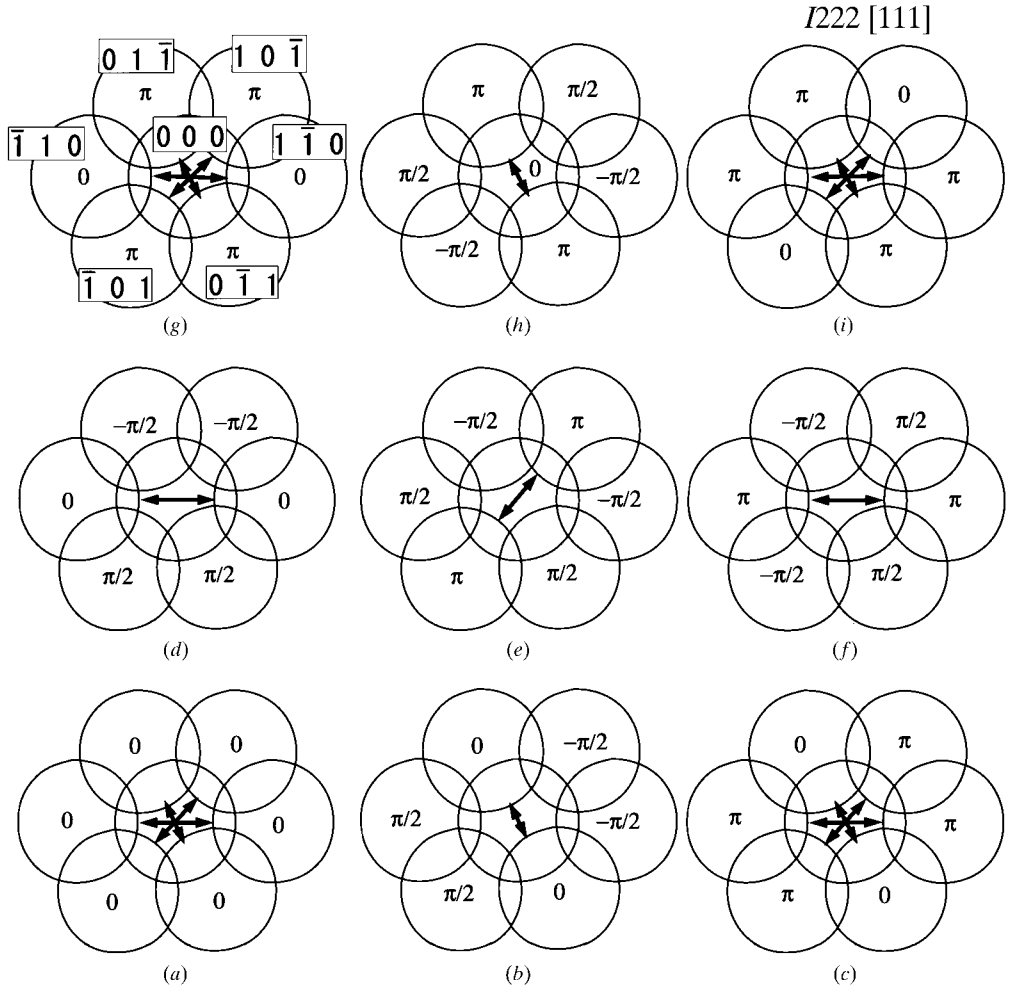

Figure 10
Phases of the kinematical crystal structure factors of the *I*222 model of Table 5 for the electron probe positions (*a*)–(*i*) illustrated in Fig. 9(*a*).

Table 5
Model structures of $I222$ and $I2_12_12_1$ used for simulations of coherent CBED patterns.

Space group	Site	(x,y,z)	Element	Lattice parameter (mm)
$I222$	8(k)	(0.05,0.10,0.15)	Si	a = 0.4, b = 0.5, c = 0.6
$I2_12_12_1$	8(d)	(0.05,0.10,0.15)	Si	a = 0.4, b = 0.5, c = 0.6

and so do the three perpendicular 2_1 axes. In contrast, a 2 axis intersects with two perpendicular 2_1 axes and a 2_1 axis intersects with two perpendicular 2 axes in $I2_13$. The difference in the intersection manner of 2 and 2_1 axes provides the distinction between the space groups. Similar to the patterns given in the previous section, we simulated [100] coherent CBED patterns consisting of zeroth-order Laue-zone (ZOLZ) reflections for the model structures of Table 3. It was found that the difference between the combination of 2 and 2_1 axes perpendicular to the incidence direction can be distinguished. However, that of the axes parallel to the incidence direction cannot be distinguished because the 2 and 2_1 axes parallel to the incidence direction show the same twofold rotation symmetry in the coherent ZOLZ CBED pattern. Thus, the [100] coherent CBED patterns cannot distinguish the space groups.

When the axes are projected along the [110] zone axis, the difference of the combinations of 2 and 2_1 axes in the [100] and [010] directions appears between $I23$ and $I2_13$. In the case of $I23$, the 2 and 2_1 axes in [100] and [010] directions are projected to different levels along the [001] axis, whereas both the 2 axes in [100] and 2_1 axes in [010] are projected to the same level along [001] in $I23$. However, when the projection of 2 and 2_1 axes along [110] or [$1\bar{1}$0] coherent ZOLZ CBED patterns are concerned, the 2 and 2_1 axes cannot be distinguished. Thus, the [110] coherent CBED patterns are useless for the distinction of the space groups.

In the above discussion, we considered only ZOLZ reflections. If we observe interference fringes between

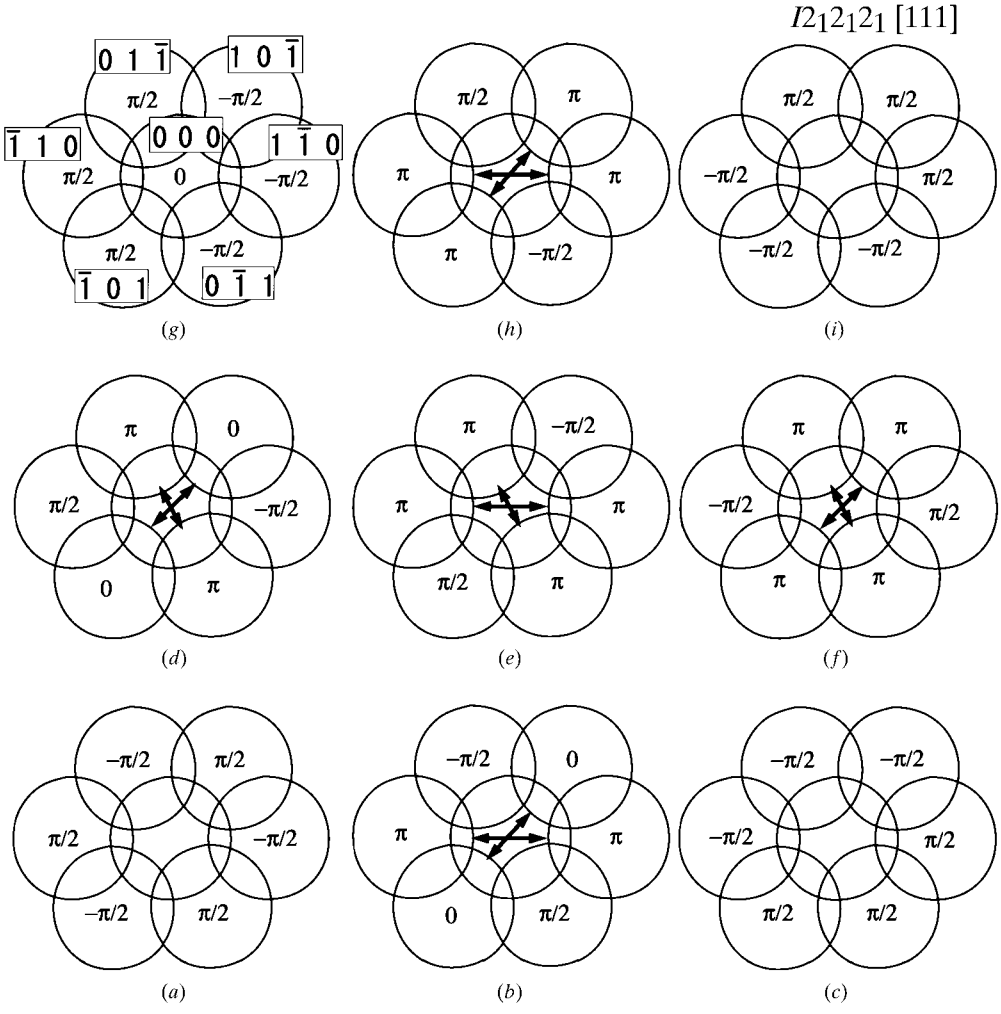

Figure 11
Phases of the kinematical crystal structure factors of the $I2_12_12_1$ model of Table 5 for the electron probe positions (*a*)–(*i*) illustrated in Fig. 9(*b*).

ZOLZ reflections and higher-order Laue-zone (HOLZ) reflections, we can examine the three-dimensional arrangements of the 2 and 2_1 axes to distinguish the space groups. However, it is difficult in practice to observe such interference fringes because such fringes have very small lattice spacings of less than 0.05 nm. Furthermore, very high coherency of the incident beam and extremely high stability in a microscope are needed to observe them.

There is another possibility to distinguish the space groups of $I23$ and $I2_13$ in the [111] coherent CBED pattern. The coherent CBED pattern shows a threefold rotation symmetry when the probe is positioned on the threefold rotation or 3_1-screw axes parallel to the [111] direction. As seen in Fig. 2, the arrangement of the 3 and 3_1 axes of $I23$ is different from that of $I2_13$. If we examine the difference in the spatial arrangement of the 3 and 3_1 axes by scanning the probe position within the unit cell, the space groups can be distinguished in principle. It is, however, technically very difficult at the present stage. In addition, the method cannot be applied to distinguish the space groups of $I222$ and $I2_12_12_1$ because they have neither 3 nor 3_1 axes.

From the above discussion, the coherent CBED method described in the previous section appears to be a feasible method to distinguish these space groups.

5. Concluding remarks

We have proposed a feasible method using coherent CBED patterns to distinguish the special pairs of space groups ($I23$ and $I2_13$) and of ($I222$ and $I2_12_12_1$), which have been indistinguishable so far. It has been shown that relative arrangements of 2 and 2_1 axes can be revealed by examining the relative phases of structure factors appearing in the interference fringes of coherent CBED patterns. We are planning to apply the method to real materials. The coherent CBED method is further expected to be used for the distinction of 3, 4 and 6 rotation axes and related screw axes, and identification of left- and right-handed space groups.

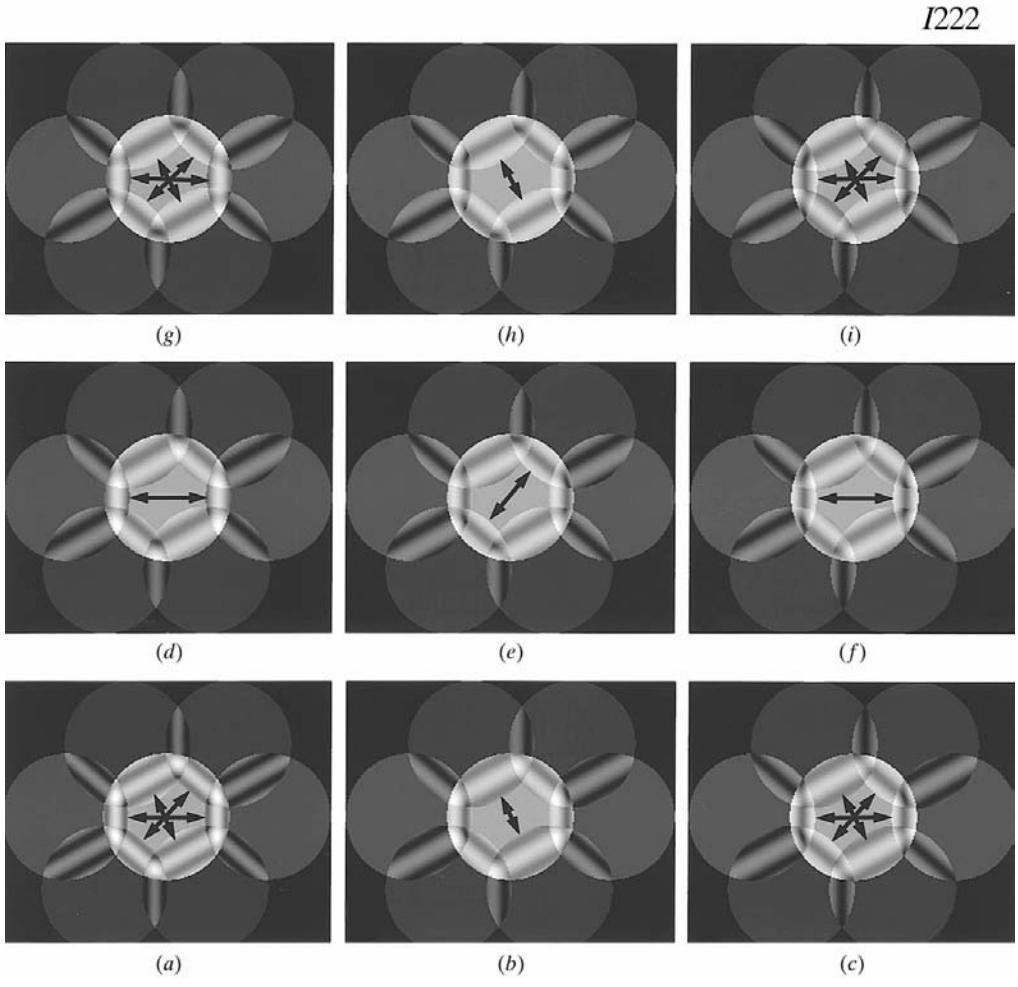

Figure 12
Coherent CBED patterns simulated for the $I222$ model of Table 5 for the electron probe positions (*a*)–(*i*) of Fig. 10.

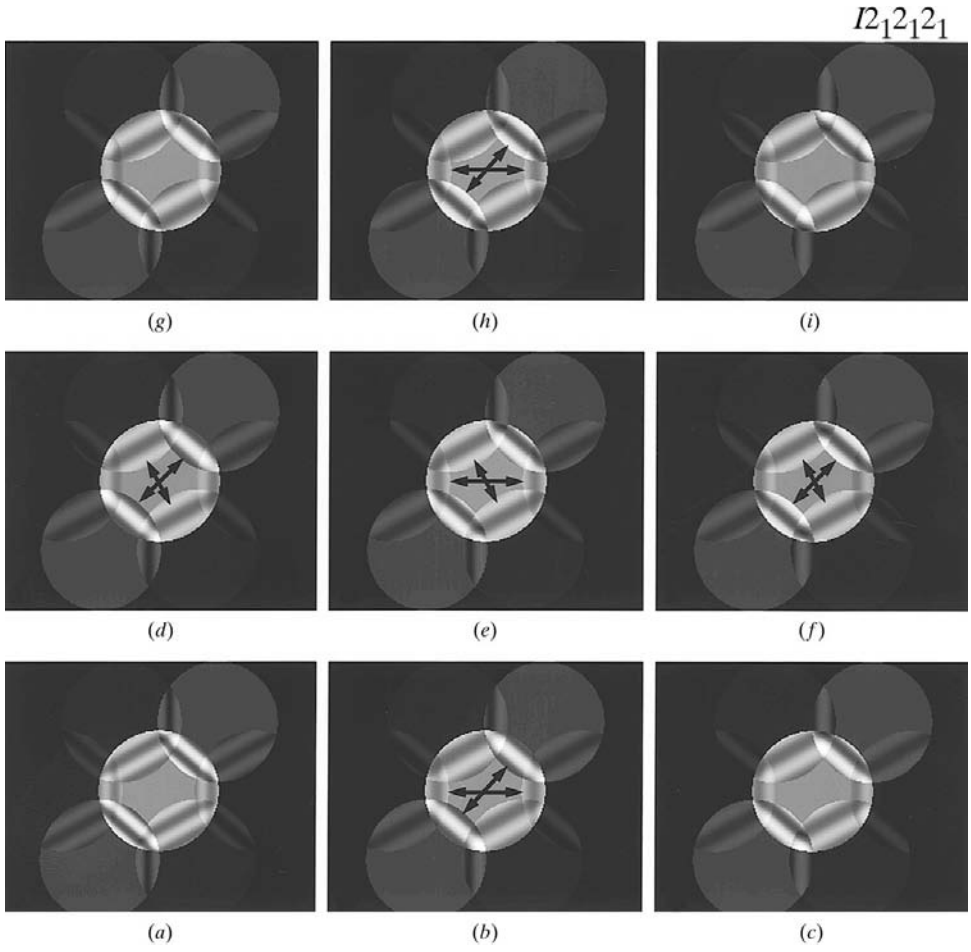

Figure 13
Coherent CBED patterns simulated for the $I2_12_12_1$ model of Table 5 for the electron probe positions (*a*)–(*i*) of Fig. 11.

This work was supported by a Grant-in-Aid for International Scientific Research (Joint Research, 10044056) from the Ministry of Education, Science, Sports and Culture of Japan.

References

Buxton, B. F., Eades, J. A., Steeds, J. W. & Rackham, G. M. (1976). *Philos. Trans. R. Soc. London*, **281**, 171–194.
Cowley, J. M. (1979). *Ultramicroscopy*, **4**, 435–450.
Dowell, W. C. T. & Goodman, P. (1973). *Philos. Mag.* **28**, 471–473.
Gjønnes, J. & Moodie, A. F. (1965). *Acta Cryst.* **19**, 65–67.
Goodman, P. (1975). *Acta Cryst.* A**31**, 804–810.
Goodman, P. & Johnson, A. W. S. (1977). *Acta Cryst.* A**33**, 997–1001.
Goodman, P. & Secomb, T. W. (1977). *Acta Cryst.* A**33**, 126.
International Tables for Crystallography (1989). Vol. A, 2nd, revised ed., edited by Th. Hahn. Dordrecht/Boston/London: Kluwer Academic Publishers.
International Tables for X-ray Crystallography (1952). Vol. I, edited by N. F. M. Henry & K. Lonsdale. Birmingham: Kynoch Press.
McCallum, B. C. & Rodenburg, J. M. (1993). *Ultramicroscopy*, **52**, 85–99.
Ou, H. J. & Cowley, J. M. (1988). Proc. 46th Annual Meeting of the Electron Microscopy Society of America, p. 882.
Spence, J. C. H. (1978). Proc. 9th International Congress on Electron Microscopy, Toronto, Canada, p. 554.
Spence, J. C. H. & Cowley, J. M. (1978). *Optik (Stuttgart)*, **50**, 129–142.
Steeds, J. W., Midgley, P. A., Spellward, P. & Vincent, R. (1995). *Electron Holography*, edited by A. Tonomura, L. F. Allard, G. Pozzi, D. C. Joy & Y. A. Ono, pp. 277–286. Amsterdam: Elsevier Science BV.
Tanaka, M. (1989). *J. Electron Microsc. Tech.* **13**, 27–39.
Tanaka, M., Saito, R. & Sekii, H. (1983). *Acta Cryst.* A**39**, 357–368.
Tanaka, M., Sekii, H. & Nagasawa, T. (1983). *Acta Cryst.* A**39**, 825–837.
Tanaka, M., Takayoshi, H., Ishida, M. & Endo, Y. (1985). *J. Phys. Soc. Jpn*, **54**, 2870–2974.
Tanaka, M. & Terauchi, M. (1985). *Convergent-Beam Electron Diffraction*. Tokyo: JEOL-Maruzen.
Tanaka, M., Terauchi, M. & Kaneyama, T. (1988). *Convergent-Beam Electron Diffraction II*. Tokyo: JEOL-Maruzen.
Tanaka, M., Terauchi, M. & Tsuda, K. (1994). *Convergent-Beam Electron Diffraction III*. Tokyo: Jeol-Maruzen.
Terauchi, M., Tsuda, K., Kamimura, O., Tanaka, M., Kaneyama, T. & Honda, T. (1994). *Ultramicroscopy*, **54**, 268–275.
Tinnappel, A. (1975). PhD thesis, Technical University, Berlin, Germany.
Tsuda, K. & Tanaka, M. (1996). *J. Electron Microsc.* **45**, 59–63.
Tsuda, K., Terauchi, M., Tanaka, M., Kaneyama, T. & Honda, T. (1994). *J. Electron Microsc.* **43**, 173–175.
Vine, W. J., Vincent, R., Spellward, P. & Steeds, J. W. (1992). *Ultramicroscopy*, **41**, 423–428.
Zuo, J. M. & Spence, J. C. H. (1993). *Philos. Mag.* **68**, 1055–1078.